Optical properties of 4H–SiC

R. Ahuja, A. Ferreira da Silva, C. Persson, J. M. Osorio-Guillén, I. Pepe et al.

Citation: J. Appl. Phys. **91**, 2099 (2002); doi: 10.1063/1.1429766
View online: http://dx.doi.org/10.1063/1.1429766
View Table of Contents: http://jap.aip.org/resource/1/JAPIAU/v91/i4
Published by the American Institute of Physics.

Optical properties of 4H–SiC

R. Ahuja[a)]
Condensed Matter Theory Group, Department of Physics, Uppsala University, P.O. Box 530, SE-751 21 Uppsala, Sweden

A. Ferreira da Silva
Instituto de Física, Universidade Federal da Bahia, Campus Universitario de Ondina 40 210 340 Salvador, Ba, Brazil

C. Persson and J. M. Osorio-Guillén
Condensed Matter Theory Group, Department of Physics, Uppsala University, P.O. Box 530, SE-751 21 Uppsala, Sweden

I. Pepe
Instituto de Física, Universidade Federal da Bahia, Campus Universitario de Ondina 40 210 340 Salvador, Ba, Brazil

K. Järrendahl, O. P. A. Lindquist, N. V. Edwards,[b)] and Q. Wahab
Department of Physics and Measurement Technology, Linköping University, SE-581 83, Linköping, Sweden

B. Johansson[c)]
Condensed Matter Theory Group, Department of Physics, Uppsala University, P.O. Box 530, SE-751 21 Uppsala, Sweden

(Received 24 May 2001; accepted for publication 30 October 2001)

The optical band gap energy and the dielectric functions of *n*-type 4H–SiC have been investigated experimentally by transmission spectroscopy and spectroscopic ellipsometry and theoretically by an *ab initio* full-potential linear muffin-tin-orbital method. We present the real and imaginary parts of the dielectric functions, resolved into the transverse and longitudinal photon moment a, and we show that the anisotropy is small in 4H–SiC. The measurements and the calculations fall closely together in a wide range of energies. © *2002 American Institute of Physics.*
[DOI: 10.1063/1.1429766]

I. INTRODUCTION

The physical properties of 4H–SiC make it an outstanding candidate for power switching device applications where Si and GaAs base devices present a very low performance.[1] The crystal has, because of its high thermal conductivity, large band gap, strong bonds, high-radiation resistance, and chemical inertness, become a prominent material for high-power, high-temperature, and high-frequency devices. Devices like field effect transistors, bipolar storage capacitors, and ultraviolet detectors have been fabricated.[2,3] Despite its technological importance, there has been so far only a few reports on the optical properties of doped the 4H polytype.[4–10]

In this article, we have investigated the optical properties of *n*-type 4H–SiC, both experimentally and theoretically. A transmission spectroscopy technique has been used for the measurement of the optical band gap energy. The dielectric functions were determined by spectroscopic ellipsometry, a powerful, nondestructive, technique for high accuracy measurements.[5,11] The calculations of the electronic structure were performed by the full-potential linear muffin-tin-orbital (FPLMTO) method.[12] The imaginary part of the dielectric function was calculated from the joint density of states and the optical matrix elements. The real part of the dielectric function was obtained by using the Kramers–Kronig transformation relation.

II. EXPERIMENTAL DETAILS

The experimental transmission spectroscopy apparatus consists of a halogen lamp used as the light source for the measurement. The polychromatic beam is diffracted by plane diffraction gratings attached to a step motor. The beam can be varied from 925 to 360 nm; a set of lens and collimator produces a monochromatic light focused onto the sample, see Ref. 13. A first order bandpass filter has been used to avoid an eventual second order contamination of the monochromatic light, which in the intrinsic resolution, obtained by the calibration process, is 1.2 nm or 0.2%. The angular spread of the beam at the sample location is 17°. Taking into account the whole equipment and analysis process, the absolute optical error associated with the systematic error gives a final total resolution of 2.8% in the energy gap determination. The light passes through the sample and is detected by a photomultiplier tube (PTM) (EMI 9558), polarized by a negative voltage from −1800 to −2200 V. The high gain and

[a)]Electronic mail: Rajeev.Ahuja@fysik.uu.se
[b)]Also at Motorola Semiconductor Products Sector, 2200 West Broadway Road, Mesa, AZ 85202.
[c)]Also at Dept. of Materials Science and Engineering, Royal Institute of Technology, SE-100 44 Stockholm, Sweden.

sensitivity of this device is enough to measure a very low photon quantity (>100). For a very opaque sample it is possible to increase the measuring sensibility (X500) connecting a very-low noise homemade amplifier to the PMT output, with no compromise of the signal to noise ratio.

The measured sample for the transmission spectroscopy experiments was *n*-type 4H–SiC, doping around 7×10^{18} cm^{-3}, with a Si-face, 25-μm-thick epilayer grown by hot wall chemical vapor deposition (CVD).[14]

The 0.7–6.5 eV ellipsometry measurements were made using a J. A. Woollam ellipsometer equipped with a compensator to increase the sensitivity in the transparent energy region (approx. <3 eV).[15] Measurements below the energy gap allowed for mathematical removal of the native oxide. Obtained SiO_2 thicknesses were compared to real-time surface over-layer removal data. Optic axes were found using reflectance difference spectroscopy. The measured samples were bulk material.[15]

The 3.5–9 eV photon energy measurements were made with a Sentech Instruments ellipsometer facilitated with MgF2 optics. The whole system was purged in nitrogen to allow measurements above 6.5 eV.[16]

III. COMPUTATIONAL METHOD

In order to study the electronic structure of 4H–SiC we have used the FPLMTO method.[12] The calculations were based on the local-density approximation (LDA) with the Hedin–Lundqvist[17] parametrization for the exchange and correlation potential. Basis functions, electron densities, and potentials were calculated without any geometrical approximation.[12] These quantities were expanded in combinations of spherical harmonic functions (with a cutoff $\ell_{\max}=8$) inside nonoverlapping spheres surrounding the atomic sites (muffin-tin spheres) and in a Fourier series in the interstitial region. The muffin-tin spheres occupied approximately 60% of the unit cell. The radial basis functions within the muffin-tin spheres are linear combinations of radial wave functions and their energy derivatives, computed at energies appropriate to their site and principal as well as orbital atomic quantum numbers, whereas outside the muffin-tin spheres the basis functions are combinations of Neuman or Hankel functions.[18,19] In the calculations reported here, we made use of valence band 3*s*, 3*p*, and 3*d* basis functions for Si and, valence band 2*s*, 2*p*, and 3*d* basis functions for C with corresponding two sets of energy parameters. The resulting basis formed a single, fully hybridizing basis set. This approach has previously proven to give a well converged basis.[12] For sampling the irreducible wedge of the Brillouin zone we used the special **k**-point method.[20] In order to speed up the convergence we have associated each calculated eigenvalue with a Gaussian broadening of width 136 meV.

IV. CALCULATION OF THE DIELECTRIC FUNCTION

The ($\mathbf{q}=\mathbf{0}$) dielectric function was calculated in the momentum representation, which requires matrix elements of the momentum, **p**, between occupied and unoccupied eigenstates. To be specific, the imaginary part of the dielectric function, $\epsilon_2(\omega)\equiv \mathrm{Im}\,\epsilon(\mathbf{q}=\mathbf{0},\omega)$, was calculated from[21]

$$\epsilon_2^{ij}(\omega)=\frac{4\pi^2e^2}{\Omega m^2\omega^2}\sum_{\mathbf{k}nn'\sigma}\langle \mathbf{k}n\sigma|p_i|\mathbf{k}n'\sigma\rangle\langle \mathbf{k}n'\sigma|p_j|\mathbf{k}n\sigma\rangle \times f_{\mathbf{k}n}(1-f_{\mathbf{k}n'})\,\delta(e_{\mathbf{k}n'}-e_{\mathbf{k}n}-\hbar\omega). \quad (1)$$

In Eq. (1), e is the electron charge, m its mass, Ω is the crystal volume and $f_{\mathbf{k}n}$ is the Fermi distribution. Moreover, $|\mathbf{k}n\sigma\rangle$ is the crystal wave function corresponding to the nth eigenvalue with crystal momentum **k** and spin σ.

With our spherical wave basis functions, the matrix elements of the momentum operator are conveniently calculated in spherical coordinates and for this reason the momentum is written $\mathbf{p}=\Sigma_\mu \mathbf{e}^*_\mu p_\mu$,[22] where μ is -1, 0, or 1, and $p_{-1}=1/\sqrt{2}\,(p_x-ip_y)$, $p_0=p_z$, and $p_1=-1/\sqrt{2}\,(p_x+ip_y)$.[23]

The evaluation of the matrix elements in Eq. (2) is done over the muffin-tin region and the interstitial separately. The integration over the muffin-tin spheres is done in a way similar to what Oppener[24] and Gashe[21] did in their calculations using the atomic sphere approximation (ASA). A full detailed description of the calculation of the matrix elements was in another article.[25] In our theoretical method the wave function [Eq. (1)] inside the muffin-tin spheres is atomic-like in the sense that it is expressed as a radial component times spherical harmonic functions (also involving the so-called structure constants), i.e.,

$$\bar{\Psi}^{\bar{k}}_{\mathrm{mt}}(\bar{r})=\sum_t c_t\bar{\chi}^{\bar{k}}_t, \quad (2)$$

where inside the sphere R' the basis function is

$$\bar{\chi}^{\bar{k}}_t=\frac{\Phi_t(\bar{r}-\bar{R})}{\Phi(S^R_{\mathrm{mt}})}\bar{\delta}_{\bar{R},R'}-\sum_{t'}\frac{\Phi_{t'}(\bar{r}-\bar{R}')}{\Phi(S^{R'}_{\mathrm{mt}})}\bar{S}^{\bar{k}}_{t,t'} \quad (3)$$

and

$$\Phi_t(\bar{r})=i^l Y^m_l(\hat{r})(\varphi(r)+\omega(D)\dot{\varphi}(r)). \quad (4)$$

In the equations above S^R_{mt} is the muffin-tin radius for atom R, $\bar{S}^{\bar{k}}_{t,t'}$ is the structure constant, D is the logarithmic derivative, $\varphi(r)$ is the numerical solution to the spherical component of the muffin-tin potential and $\dot{\varphi}(r)$ is the energy derivative of $\varphi(r)$.[18,19] Therefore, this part of the problem is quite analogous to the ASA calculations[21,24] and we calculate the matrix elements in Eq. (2) as

$$\langle \mathbf{k}n\sigma|p_\mu|\mathbf{k}n'\sigma\rangle=\sum_{t,t'}c_t c^*_{t'}\langle\chi_{t'}|p_\mu|\chi_t\rangle. \quad (5)$$

Since, χ_t involves a radial function multiplied with a spherical harmonic function, i.e., $f(r)Y^m_l$ (we will label this product $|l,m\rangle$), we can calculate the matrix elements in Eq. (5) using the relations

$$\langle l+1,0|p_0|l,0\rangle=\frac{l+1}{\sqrt{(2l+1)(2l+3)}}\left\langle f^*(r)\left(\frac{\delta}{\delta r}-\frac{l}{r}\right)f(r)\right\rangle \quad (6)$$

and

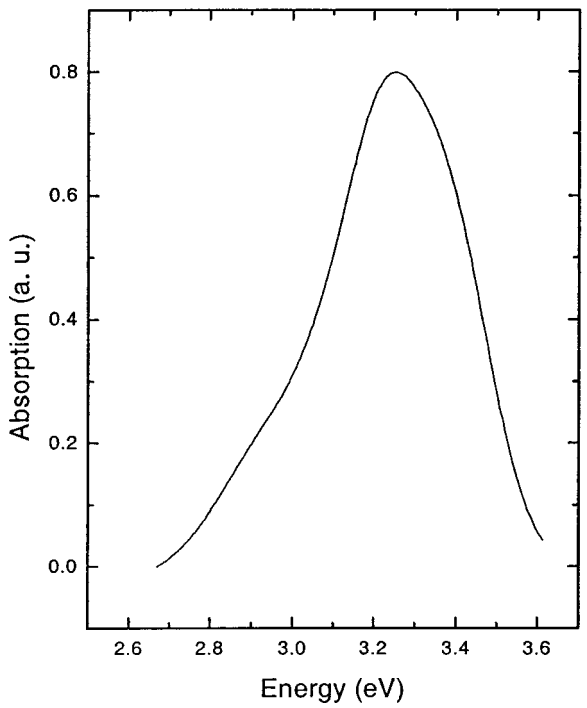

FIG. 1. Absorption spectrum intensity of *n*-type doped 4H–SiC as a function of photon energy.

$$\langle l-1,0|p_0|l,0\rangle = \frac{l}{\sqrt{(2l-1)(2l+1)}} \times \left\langle f^*(r)\left(\frac{\delta}{\delta r}+\frac{l+1}{r}\right)f(r)\right\rangle. \quad (7)$$

A general matrix element, $\langle l',m'|p_i|l,m\rangle$is then calculated using the Wigner–Eckart theorem.[22] Matrix elements of the momentum over the interstitial are obtained from the relation

$$\int_{\Omega_{\rm int}} d^3r(\psi_i^*\nabla\psi_j) = \frac{1}{\kappa_j^2}\int_{\Omega_{\rm int}} d^3r(\psi_i^*\nabla^2\nabla\psi_j). \quad (8)$$

By use of Green's second theorem the expression above can be expressed as

$$\int_{\Omega_{\rm int}} d^3r(\psi_i^*\nabla^2\nabla\psi_j) = -\int_{S_{\rm MT}} dS\left(\psi_i^*\nabla\frac{d}{dr}\psi_j\right). \quad (9)$$

In the expression above the surface integral is taken over the muffin-tin spheres and, since the interstitial wave function by construction is the same as the muffin-tin wave function, we can use for ψ the numerical wave function defined inside (and on the boundary of) the muffin-tin spheres. In this way the evaluation of the integral above is done in quite a similar way as done for the muffin-tin contribution [Eqs. (6)–(8)] to the gradient matrix elements.

The summation over the Brillouin zone in Eq. (1) is calculated using linear interpolation on a mesh of uniformly distributed points, i.e., the tetrahedron method. Matrix elements, eigenvalues, and eigenvectors are calculated in the irreducible part of the Brillouin zone. The correct symmetry for the dielectric constant was obtained by averaging the calculated dielectric function. Finally, the real part of the dielectric function, $\epsilon_1(\omega)$, is obtained from $\epsilon_2(\omega)$ using the Kramers–Kronig transformation

$$\epsilon_1(\omega) \equiv \mathrm{Re}(\epsilon(\mathbf{q}=0,\omega)) = 1+\frac{1}{\pi}\int_0^\infty d\omega'\,\epsilon_2(\omega') \times\left(\frac{1}{\omega'-\omega}+\frac{1}{\omega'+\omega}\right). \quad (10)$$

V. RESULTS

Figure 1 shows the room temperature absorption spectrum for the *n*-type doped 4H–SiC as a function of photon energy. The optical band gap energy is evaluated from the peak position of the absorption. The value obtained is $E_g = 3.260 \pm 0.098$ eV. The band gap value of about 3.27 eV for

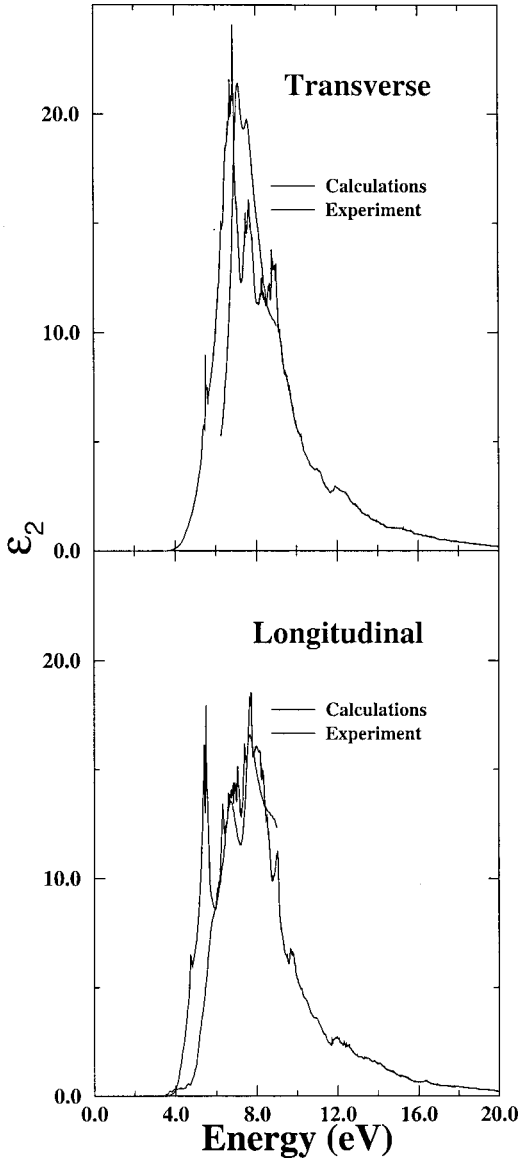

FIG. 2. The transverse $\perp$ (upper panel) and the longitudinal $\parallel$ (lower panel) components of the imaginary part ϵ_2 of the dielectric function.

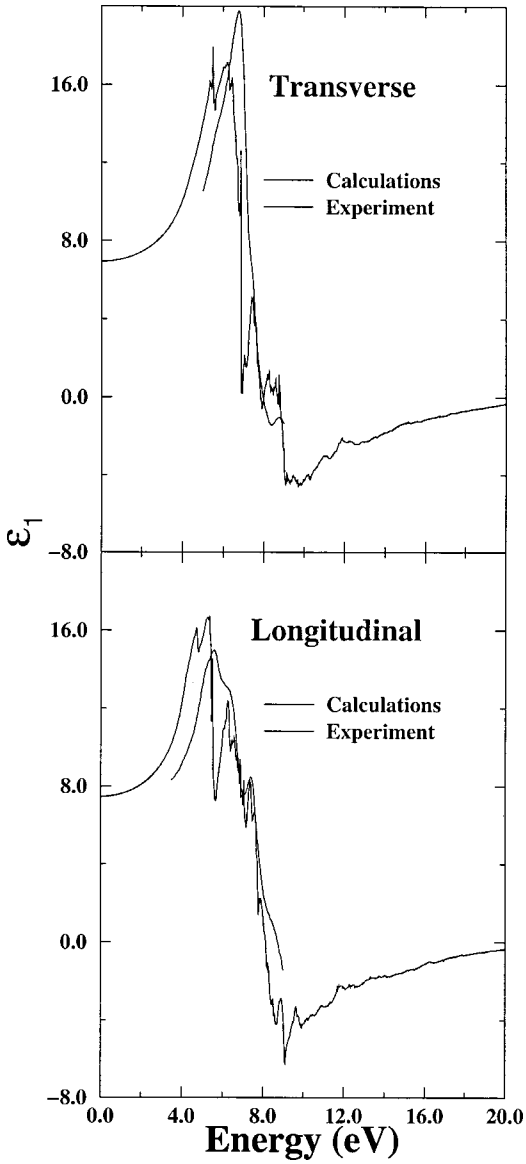

FIG. 3. The transverse $\perp$ (upper panel) and the longitudinal $\parallel$ (lower panel) components of the real part ϵ_1 of the dielectric function.

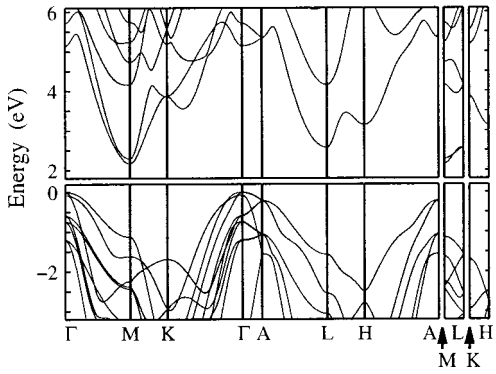

FIG. 4. The electronic structure of 4H–SiC.

intrinsic material at room temperature[26,27] will be lower in energy due to screening of the temperature-induced excitations of electrons. For an impurity concentration of 7×10^{18} cm^{-3}, the free electron concentration is about 5×10^{17} cm^{-3},[28,29] and with this gas of free electrons the band gap is reduced by about 40 meV,[6,7] yielding a band gap of about 3.23 eV. This is very close to the present measured value.

The measured transverse ($\perp$) and longitudinal ($\parallel$) imaginary part of the dielectric function, $\epsilon_2^{\perp}$ and $\epsilon_2^{\parallel}$, of the doped 4H–SiC, are shown in Fig. 2 in the 0.9–7.0 eV photon range energy, together with the theoretical results. In Fig. 3, we show the corresponding real part of the dielectric function, $\epsilon_1^{\perp}$ and $\epsilon_1^{\parallel}$.

The electronic structure of intrinsic 4H–SiC is shown in Fig. 4. The conduction-band minimum is located at the *M* point and the calculated band gap is 2.22 eV, which is about 30% below the experimental value of 3.29 eV.[27] It is well known that LDA underestimates the band gap in semiconductors and insulators, however, it is believed that the optical properties can be described accurately by the LDA.

Also, the second lowest conduction-band minimum is located at the *M* point, separated by only 120 meV from the lowest minimum. This energy difference is close to the energy of the optical phonon energies of 0.104–0.121 eV,[27] and the second band will therefore influence the transport properties at high temperatures or for high applied electric fields.

In Fig. 5, we show the calculated partial density of states (DOS) of 4H–SiC. The particular choice of Si or C atom is immaterial, since all Si or C atoms in the unit cell have very similar partial DOS. In the figure, one can see that the valence band, as expected, consists of two subbands. The lower-lying subband is in the range from about -15.5 to -10 eV and is dominated by the atomic Si $3s+3p$ states and the localized atomic C $2s$ states, whereas the higher subband also consists of Si $3d$ and C $2p$ states. In the higher subband the Si $3s$ and C $2p$ states dominate at lower energies and the C $2p$ states dominate at higher energies. Even if it is not straightforward to compare x-ray spectra with the DOS, the clear peak at about -7.1 eV, arising from the atomic C $2p$ and Si $3s$ states, can probably be identified with the experimental value -8.5 eV.[30] Also the total bandwidth and the width of the higher subband seem to be underestimated in the LDA calculation. The calculated width of the total band (higher subband) is about 15.5 (8.5) eV, whereas the experimental result is about 18.2 (10.0) eV.[30]

From the electronic structure and the partial DOS we can identify the optical absorption, described by the imaginary part of the dielectric function (Fig. 2). Here, we should consider the correction of the band gap of $\Delta E_g = 1.07$ eV, which shifts the calculated $\epsilon_2(\omega)$ upwards in photon energy. With the band gap correction, the agreement between the calculations and the measurements is excellent. The absorption starts at about 4.0 eV with optical transitions about the *M* point. For energies between 4.0 and 5.5 eV we can address the absorption to transitions along the *ML* line, which is consistent with calculation of Adolph *et al.*[31] The peak at 6.2 for the longitudinal direction comes from optical transitions at the Γ points, whereas the peaks at 6.7, 7.8 for both directions come, most likely, from transitions about the *L* and *K* points, respectively.

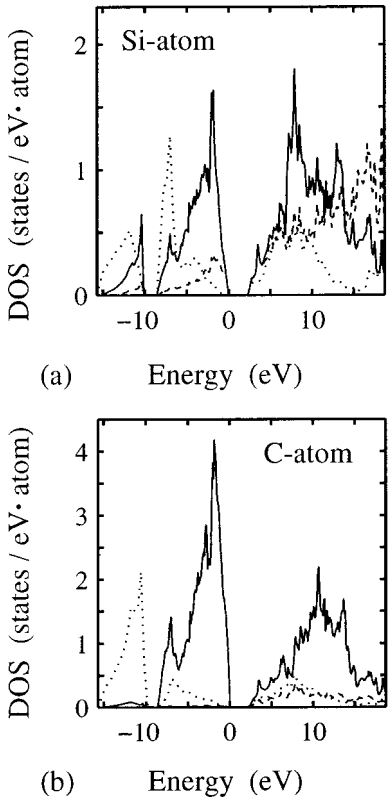

FIG. 5. The partial DOS of (a) Si and (b) C atom. Dotted, solid, and dashed lines represent *s*, *p*, and *d* states, respectively.

There is also very good agreement between the measured and the calculated real part of the dielectric function after the band gap correction has been included. The calculated ''high''-energy limit of the dielectric function, $\epsilon_1(\infty)$, is 6.94 and 7.47 for the transverse and longitudinal directions, respectively, and, thus, the optical anisotropy is small in 4H–SiC. The calculated dielectric constants are slightly larger than the corresponding experimental values of 6.52 and 6.70, respectively.[26] This is in correspondence with the underestimate of the band gap.

VI. CONCLUSIONS

We have measured the optical properties of 4H–SiC, using transmission spectroscopy and spectroscopic ellipsometry. The resulting dielectric functions are in excellent agreement with our full-potential calculations. We have identified the optical transitions from the partial DOS and the electronic structure, as being transitions along the *ML* line and at the Γ, *L*, and *K* points. By comparing the dielectric function in the transverse and longitudinal directions, we conclude that the optical anisotropy is small in 4H–SiC.

ACKNOWLEDGMENTS

This work was financially supported by TFR, NFR, SSF, and the Brazilian National Research Council (CNPq).

[1] R. J. Trew, J. Yan, and P. M. Mock, Proc. IEEE **79**, 598 (1991).
[2] H. Morkoc, S. Strite, G. B. Gao, M. E. Lin, B. Sverdlov, and M. Burns, J. Appl. Phys. **76**, 1363 (1994).
[3] J. W. Palmour, J. A. Edmond, H. S. Kong, and C. H. Carter, Jr., Physica B **185**, 461 (1993).
[4] E. Janzén and O. Kordina, Mater. Sci. Eng., B **46**, 203 (1997).
[5] S. Zollner, J. G. Chen, E. Duda, T. Wetteroth, S. R. Wilson, and J. N. Hilfiker, J. Appl. Phys. **85**, 8353 (1999).
[6] C. Persson, U. Lindefelt, and B. E. Sernelius, J. Appl. Phys. **86**, 4419 (1999).
[7] C. Persson, U, Lindefelt, and B. E. Sernelius, Phys. Rev. B. **60**, 16479 (1999).
[8] C. Limpijumnong, W. R. L. Lambrecht, S. N. Rashkeev, and B. Segall, Phys. Rev. B **59**, 12890 (1999).
[9] O. P. A. Lindquist, H. Arwin, U. Forsberg, J. P. Bergman, and K. Järrendhal, Mater. Sci. Forum **338–342**, 575 (2000).
[10] R. Jansson, S. Zangooie, H. Arwin, and K. Järrendahl, Phys. Status Solidi B **218**, R1 (2000).
[11] S. Zangooie, P. O. A. Persson, J. N. Hilfiker, L. Hultman, and H. Arwin, J. Appl. Phys. **87**, 8497 (2000).
[12] J. M. Wills (unpublished); J. M. Wills and B. R. Cooper, Phys. Rev. B **36**, 3809 (1987); D. L. Price and B. R. Cooper, *ibid.* **39**, 4945 (1989).
[13] C. Moysés Araújo, J. Souza de Almeida, I. Pepe, A. Ferreira da Silva, Bo E. Sernelius, J. P. de Souza, and H. Boudinov, Phys. Rev. B **62**, 12882 (2000).
[14] Q. Wahab, A. Ellison, A. Henry, E. Janzén, C. Hallin, J. Di Persio, and R. Martinez, Appl. Phys. Lett. **76**, 2725 (2000).
[15] N. V. Edwards, K. Järrendahl, K. Robbie, G. Powell, D. E. Aspnes, C. Cobet, N. Esser, W. Richter and L. D. Madsen, Surf. Sci. Lett. (in print).
[16] O. P. A. Lindquist, K. Järrendahl, S. Peters, J.-T. Zettler, C. Cobet, N. Esser, and D. E. Aspnes, Appl. Phys. Lett. **78**, 2751 (2001).
[17] L. Hedin and B. I. Lundqvist, J. Phys. C **4**, 2064 (1971).
[18] O. K. Andersen, Phys. Rev. B **12**, 3060 (1975).
[19] H. L. Skriver, *The LMTO Method* (Springer, Berlin, 1984).
[20] D. J. Chadi and M. L. Cohen, Phys. Rev. B **8**, 5747 (1973); S. Froyen, Phys. Rev. B **39**, 3168 (1989).
[21] A good description of the calculation of dielectric constants and related properties is found in the thesis by T. Gashe, Uppsala University, 1993.
[22] A. R. Edmonds, *Angular Momentum in Quantum Mechanics* (Princeton University Press, Princeton, NJ, 1974).
[23] In practice we calculate matrix elements of the symmetrized momentum operator $\langle i|\vec{\mathbf{p}}_\mu|j\rangle \equiv (\langle i|p_\mu j\rangle + (-1)^\mu \langle p_{-\mu} i|j\rangle)/2$.
[24] P. M. Oppeneer, T. Maurer, J. Sticht, and J. Kübler, Phys. Rev. B **45**, 10924 (1992).
[25] R. Ahuja, S. Auluck, J. M. Wills, M. Alouani, B. Johansson, and O. Eriksson, Phys. Rev. B **55**, 4999 (1997).
[26] W. J. Coyke, Mater. Res. Bull. **4**, 141 (1969).
[27] *Properties of Silicon Carbide*, edited by G. L. Harris (INSPEC, London, 1995).
[28] C. Persson and U. Lindefelt, *Proceedings of the 7th International Conference on Silicon Carbide, III-Nitrides, and Related Materials*, edited by G. Pensl *et al.* (Trans Tech, Uetikon-Zürich, 1998), Vols. 264–268.
[29] C. Persson and U. Lindefelt, J. Appl. Phys. **83**, 266 (1998).
[30] I. I. Zhukova, V. A. Fomichev, A. S. Vinogradov, and T. M. Zimkina, Sov. Phys. Solid State **10**, 1097 (1968).
[31] B. Adolph, K. Tenelsen, V. I. Gavrilenko, and F. Bechstedt, Phys. Rev. B **55**, 1422 (1997).